




A new Centiloid method for ^{18}F -florbetaben and ^{18}F -flutemetamol PET without conversion to PiB

Soo Hyun Cho^{1,2} · Yeong Sim Choe^{1,3,4} · Hee Jin Kim^{1,4} · Hyemin Jang^{1,4} · Yeshin Kim^{1,5} · Si Eun Kim^{1,6} · Seung Joo Kim^{1,7} · Jun Pyo Kim^{1,4} · Young Hee Jung^{1,8} · Byeong C. Kim² · Suzanne L. Baker⁹ · Samuel N. Lockhart¹⁰ · Duk L. Na^{1,3,4,11} · Seongbeom Park^{1,4} · Sang Won Seo^{1,3,4,12,13,14} 

Received: 7 June 2019 / Accepted: 4 November 2019 / Published online: 13 December 2019

© Springer-Verlag GmbH Germany, part of Springer Nature 2020

Abstract

Purpose We developed a new method to directly calculate Centiloid (CL) units of ^{18}F -florbetaben (FBB) and ^{18}F -flutemetamol (FMM) without conversion to the PiB standardized uptake value ratio (SUVR).

Methods Paired FBB and FMM PET scans were obtained from 20 Alzheimer's disease-related cognitive impairment patients, 16 old controls, and 20 young controls. We investigated the correlations between the FBB and FMM CL units using the direct comparison of FBB-FMM CL (dcCL) method and the standard CL method and compare differences in FBB and FMM CL units between dcCL method and the standard method.

Results Following the conversion of FBB or FMM SUVRs into CL units, a direct relationship was formed between the FBB or FMM SUVRs and the CL units using dcCL method (FBB dcCL = $151.42 \times \text{FBB dcSUVR} - 142.24$ and FMM dcCL = $148.52 \times \text{FMM dcSUVR} - 137.09$). The FBB and FMM CL units were highly correlated in both our method ($R^2 = 0.97$, FMM dcCL = $0.97 \times \text{FBB dcCL} + 1.64$) and the standard method ($R^2 = 0.97$, FMM CLstandard = $0.79 \times \text{FBB CLstandard} + 1.36$). However, the CL variations between FBB and FMM were smaller when calculated by dcCL method (6.15) than when calculated by the previous method (10.22; $P = 0.01$).

Conclusions Our findings suggest that our direct comparison of FBB-FMM method, rather than the standard method, is a reasonable way to convert FBB or FMM SUVRs into CL units, at least in environments where FBB or FMM ligands are used frequently.

Keywords Florbetaben · Flutemetamol · Centiloid · Amyloid imaging · Standardization · Alzheimer's disease

Soo Hyun Cho and Yeong Sim Choe contributed equally to this article as co-first authors.

Seongbeom Park and Sang Won Seo contributed equally to this article as co-corresponding authors.

This article is part of the Topical Collection on Neurology

Electronic supplementary material The online version of this article (<https://doi.org/10.1007/s00259-019-04596-x>) contains supplementary material, which is available to authorized users.

✉ Seongbeom Park
ayl1815@gmail.com

✉ Sang Won Seo
sangwonseo@empal.com

Extended author information available on the last page of the article

Introduction

The use of amyloid beta ($\text{A}\beta$) PET imaging technology to detect diagnostic and predictive biomarkers of Alzheimer's disease (AD) has increased greatly in recent years. The first publication of an $\text{A}\beta$ -selective imaging agent, ^{11}C -labeled Pittsburgh compound B (^{11}C -PiB) [1], opened the door to in vivo detection of a fundamental aspect of AD pathology. The limitation of the short half-life (20 min) of ^{11}C -PiB prompted the development and commercialization of ^{18}F -labeled $\text{A}\beta$ imaging agents, such as ^{18}F -florbetapir [2], ^{18}F -florbetaben (FBB) [3], and ^{18}F -flutemetamol (FMM) [4], which has allowed greater distribution and use of $\text{A}\beta$ PET imaging in many hospitals with PET centers. To the best of our knowledge, no head-to-head comparison of the ^{18}F ligands has yet been conducted. However, previous studies showed that PiB uptake correlates highly with the uptakes of those three ^{18}F ligands [5–7].

Each tracer has its own unique dynamics and kinetics. Previous studies that have quantitatively evaluated and compared multiple tracers in the same participants have used different cortical targets [8], reference regions [5], methods for evaluation [9, 10], and positive PET cut-off points [5]. Consequently, there is a need to standardize the methods for data collection and analysis to improve cross-center, multi-tracer utility. In this regard, an international working party of A β imaging researchers developed a method to standardize quantitative A β imaging measures by scaling the outcome to the Centiloid (CL) unit using the PiB ligand [11]. This unit has a zero CL point that corresponds to the mean result from scans in young adults who are estimated to be free of A β plaques. The 100 CL point corresponds to the mean result of scans performed in a group of participants with typical AD of mild severity, the time of the highest A β burden in the course of AD [11, 12].

CL methods and scaling factors for ^{18}F -labeled A β tracers have recently been published [6, 7, 13], allowing the comparison of tracer characteristics relative to PiB under strictly controlled head-to-head conditions. These methods enable ^{18}F -labeled A β tracers to be converted into CL units without the need for paired PiB scans. Because ^{18}F ligands are increasingly replacing PiB in both clinical and research settings, the need is growing for appropriate standardization of the ^{18}F ligands themselves for common use and comparison. However, given that the CL units calculated for any ^{18}F tracers have one more degree of separation than those for PiB, the comparison of two or more ^{18}F A β tracers in CL units would suffer from the limitations of a second degree of separation. That is, converting ^{18}F A β tracer uptake to CL via PiB could introduce differences into the process because the unique characteristics of PiB might influence the CL scale.

Therefore, in the present study, we conducted head-to-head comparisons of A β PET imaging using the FBB and FMM ligands in younger control (YC), older control (OC), and AD-related cognitive impairment (ADCI) participants. We also converted the standardized uptake volume ratio (SUVR) of FMM and FBB into CL units using both our new direct comparison of FBB-FMM CL (dcCL) method, which directly calculates the CL units from the SUVRs of FBB and FMM without conversion through the PiB SUVR, and the standard method, which requires translation into the PiB SUVR. First, we investigated the correlation of CL units between FBB and FMM using the two CL derivation methods. Second, we compared the differences in CL units of FBB and FMM calculated by our dcCL method and the standard CL method. We hypothesized that the CL units between FBB and FMM would be highly correlated. We also hypothesized that the differences in CL units of FBB and FMM would be smaller when calculated with our dcCL method than with the standard CL method.

Materials and methods

Participants

We recruited 20 YC, 16 OC, and 20 ADCI participants. All participants underwent magnetic resonance imaging (MRI) and A β PET with both FBB and FMM. In this study, we combined 16 AD dementia and 4 amnesic mild cognitive impairment (aMCI) patients who were all A β PET positive (+) into the ADCI group [14]. AD dementia was diagnosed based on the National Institute on Aging-Alzheimer's Association research criteria for probable AD [15]. To be diagnosed with aMCI, participants had to meet Petersen's criteria [16] and show objective memory impairment one standard deviation below the norm in at least one memory test. OCs, defined as those older than 65 years (age [mean \pm standard deviation], 74.0 \pm 3.6 years), were all characterized by the following: (1) no history of neurologic or psychiatric disorders, (2) normal cognitive function determined using neuropsychological tests, and (3) a negative (–) A β PET image. Healthy YCs, defined as those younger than 40 years (32.0 \pm 3.9 years), had (1) no history of neurologic or psychiatric disorders, (2) normal cognitive function (Mini-Mental State Examination [MMSE] score, 29.9 \pm 0.4), and (3) A β (–) PET results.

All participants were evaluated by clinical interview and neurological and neuropsychological examinations and underwent laboratory tests (complete blood count, blood chemistry, vitamin B12/folate, syphilis serology, and thyroid function). Brain MRI confirmed the absence of structural lesions, including territorial cerebral infarctions, brain tumors, hippocampal sclerosis, and vascular malformations.

This study protocol was approved by the Institutional Review Board of Samsung Medical Center. We obtained written consent from each participant, and all methods were carried out in accordance with the approved guidelines.

MRI data acquisition

We acquired standardized three-dimensional T1 turbo field echo images from all participants at Samsung Medical Center, using the same 3.0-T MRI scanner (Philips Achieva; Philips Healthcare, Andover, MA, USA), with the following parameters: sagittal slice thickness, 1.0 mm over contiguous slices with 50% overlap; no gap; repetition time of 9.9 ms; echo time of 4.6 ms; flip angle of 8°; and matrix size of 240 \times 240 pixels reconstructed to 480 \times 480 over a field of view of 240 mm [17].

A β PET data acquisition

Participants underwent FBB PET and FMM PET at Samsung Medical Center using a Discovery S $\text{T}e$ PET/CT scanner (GE

Medical Systems, Milwaukee, WI, USA) in three-dimensional scanning mode that examined 47 slices of 3.3-mm thickness spanning the entire brain [18, 19]. Paired FBB and FMM PET images were acquired on two separate days; there were no differences in mean interval times (4.0 ± 2.5 months across all groups) among the three groups ($P = 0.89$). We performed FBB PET first in half of the participants (total 29: 8 ADCL, 12 OC, and 9 YC) and FMM PET first in the other half (total 27: 12 ADCL, 4 OC, and 11 YC). CT images were acquired using a 16-slice helical CT (140 KeV, 80 mA; 3.75-mm section width) for attenuation correction. According to the protocols proposed by the ligands' manufacturers, a 20-min emission PET scan with dynamic mode (consisting of 4×5 min frames) was performed 90 min after injection of a mean dose of 311.5 MBq of FBB or 185 MBq of FMM. Three-dimensional (3D) PET images were reconstructed in a $128 \times 128 \times 48$ matrix with a voxel size of $2 \text{ mm} \times 2 \text{ mm} \times 3.27 \text{ mm}$ using the ordered-subsets expectation maximization algorithm (FBB iterations = 4 and subset = 20; FMM iterations = 4 and subset = 20).

All PET images were reviewed by nuclear medicine physicians who were blinded to patient information and diagnosed classification, and they were dichotomized as A β positive or negative using visual reads on the standardized scoring systems [20, 21].

Imaging analysis

We replicated the image processing steps described in the previously published Centiloid Project [11]. Each participant's MRI image was co-registered to the MNI-152 template, and then each participant's PET image was co-registered via the derived MRI transformation parameters using the SPM8 unified segmentation method, as described in detail in the CL methodology paper [11]. We used T1-weighted MR-image correction with the N3 algorithm only for intensity non-uniformities [22]. No corrections were applied to the PET images for brain atrophy or partial volume effects. We downloaded the whole cerebellum (WC) mask and standard CL global cortical target volume of interest (CTX VOI) from the Global Alzheimer's Association Interactive Network (GAAIN) website (<http://www.gaain.org>).

Standard and FBB-FMM Global CTX VOI

The FBB-FMM CTX VOI was generated by using SUVR parametric images (with the WC reference VOI) from the 20 typical ADCL patients (AD-CTX), who were also used in the CL scaling described below, as well as the 16 OCs (OC-CTX). To generate the FBB-FMM CTX VOI, the average OC-CTX image was subtracted from the average AD-CTX image, and then we defined the FBB-FMM CTX VOI as areas of AD-

related brain A β accumulation common to both FBB and FMM PET. To extract the FBB-FMM CTX VOI, we first obtained the FBB CTX VOI and the FMM CTX VOI and then found the intersection of those images. After that, only the upper 20% of the intersecting images was used as the FBB-FMM CTX VOI [23]. We smoothed those regions with a 3D-Gaussian filter with a full width at half maximum of 8.0 mm to retain regions similar to the published CTX ROI [11]. Individual SUVR values in the FBB-FMM CTX VOI were calculated using the WC as a reference region. The standard CTX VOI was also calculated as the ratio of cortical to WC SUVR using the standard CTX and WC VOIs downloaded from GAAIN.

Centiloid units

As part of our direct comparison of FBB-FMM conversion method, we directly converted the SUVR values of the FBB-FMM CTX VOI into dcCL units using the CL conversion equation [11]:

$$CL = 100 \times (SUVR_{ind} - SUVR_{YC-0}) / (SUVR_{ADCL-100} - SUVR_{YC-0})$$

where $SUVR_{ind}$ represents the individual SUVR values of all YC-0 and ADCL-100 participants, and $SUVR_{YC-0}$ and $SUVR_{ADCL-100}$ represent each group's mean SUVR values. The CL equation was derived separately for FBB and FMM PET and applied to the FBB and FMM SUVR, respectively, from the FBB-FMM CTX VOI. We named SUVR from the FBB-FMM CTX VOI used to make dcCL as dcSUVR.

To acquire standard CL units using the standard CTX VOI, we first calculated the $SUVR_{standard}$ using the WC as a reference and then calculated the FBB and FMM $CL_{standard}$ values using the CL transformation equation derived from previous studies of FBB ($FBB \text{ } CL_{standard} = 153.4 \times FBB \text{ } SUVR_{standard} - 154.9$) [6] and FMM ($FMM \text{ } CL_{standard} = 121.42 \times FMM \text{ } SUVR_{standard} - 121.16$) [7].

Statistical analysis

To compare demographic characteristics, we used the analysis of variance for continuous variables and chi-square testing for categorical variables. We also performed a linear regression to assess correlations between the cortical retention values for each pair of tracers. Because the sample size is larger than 30, we can assume that the CL unit and SUVR represent a normal distribution using the central limit theorem in the regression analysis.

The effect size was calculated with the following equation:

$$\text{Effect Size} = (\mu_p - \mu_n) / \sqrt{(N_p \sigma_p^2 + N_n \sigma_n^2) / (N_p + N_n - 2)}$$

where μ_p and μ_n are the average SUVR in the ADCI and YC groups.

σ_p^2 and σ_n^2 are the variance of the ADCI and YC groups.

N_p and N_n are the number of participants in the ADCI and YC groups.

The variability in the YC cohort mainly reflects the noise from each method, so low variability within the YC cohort indicates low noise in pathology-free scans. To find the within-group variability for each ligand, we performed Levene's test for equal variance. We demonstrated a CL unit difference between FBB and FMM using Bland-Altman plots [24] of both our direct comparison method and the standard method. The FBB and FMM CL values in the ADCI and YC groups follow the normal distribution, as shown by the Shapiro-Wilk test for each group, in the direct comparison of FBB-FMM method (ADCI: $W = 0.97$ ($P = 0.68$), YC: $W = 0.98$ ($P = 0.87$)) and the standard method (ADCI: $W = 0.96$ ($P = 0.64$), YC: $W = 0.98$ ($P = 0.89$)). However, the combined ADCI and YC groups did not follow the normal distribution with either method (direct comparison of FBB-FMM method: $W = 0.84$ ($P < 0.001$), standard method: $W = 0.85$ ($P < 0.001$)). We compared the absolute value differences in CL units: (1) between FBB CL and FMM CL derived by our direct comparison of FBB-FMM method and the standard method and (2) between our direct comparison method and the standard method for calculating FBB CL and for FMM CL. To find the smaller absolute value differences in the CL units, we used a generalized estimating equation (GEE). We used SPSS version 24.0 (SPSS Inc., Chicago, IL, USA) for the chi-square tests, linear regression, Levene's test, and GEE, and we used MedCalc Statistical Software version 17.9.2 (Ostend, Belgium; 2017) for the Bland-Altman plots.

Results

Replicate analysis using GAAIN PiB data in standard CTX VOI

To validate our local standard CL process pipeline using GAAIN PiB data, we calculated SUVR values using the standard CTX VOI. We found excellent correlation ($CL_{our} = 1.00 \times CL_{GAAIN} - 0.08$; $R^2 = 0.99$, slope 1.00, intercept -0.08), well within the range considered to replicate previous findings ($R^2 > 0.98$, slope 0.98–1.02, intercept between -2 and $+2$); thus, our image registration and measurement processes were valid within the acceptance criteria defined by Klunk et al. [11].

Participant demographics

Table 1 shows the demographic information of the participants. The OC participants (age mean \pm SD: $74.0 \pm$

Table 1. Participant demographics and clinical findings

	A β (+) ADCI	A β (–) OC	A β (–) YC
Number of participants	20	16	20
Sex (M/F)	9/11	6/10	11/9
Age, years (mean \pm SD)	67.2 ± 8.2	$74.0 \pm 3.6^{a,b}$	$32.0 \pm 3.9^{a,b}$
MMSE (mean \pm SD)	19.2 ± 7.0	26.9 ± 2.1^a	29.9 ± 0.4^a
APOE ϵ 4, no. (%)	16 (80)	3 (18.8) ^a	3 (15) ^a

A β , amyloid beta; ADCI, Alzheimer's disease-related cognitive impairment; OC, old control; YC, young control; MMSE, Mini-Mental State Examination; APOE ϵ 4, apolipoprotein E ϵ 4 allele; SD, standard deviation; M/F, male/female

Statistical analyses used chi-square tests for sex and APOE ϵ 4. Analysis of variance was used for age and MMSE

^a $P < 0.05$ between A β (+) ADCI and A β (–) OC or A β (–) YC

^b $P < 0.05$ between A β (–) OC and A β (–) YC

3.6 years) were older than the ADCI participants (67.2 ± 8.2 years). There were no differences in sex proportions among the groups. The MMSE score (mean \pm SD) of the A β (–) OCs was 26.9 ± 2.1 and that of the A β (–) YCs was 29.9 ± 0.4 . There were significant differences in the MMSE scores between the ADCI participants and both the OCs and YCs, but there was no significant difference between the OCs and YCs. The frequency of APOE ϵ 4 carriers was 80% in the A β (+) ADCI participants, 18.8% in the A β (–) OCs, and 15% in the A β (–) YCs.

Correlation of SUVRs between FMM and FBB

Figure 1 shows the group-averaged differences between the ADCI participants and OCs using FBB (Fig. 1a) and FMM (Fig. 1b), indicating the areas of AD-related A β deposition. The spatial distribution of A β deposition in the FBB-FMM CTX VOI did not seem to differ between FBB and FMM. The FBB-FMM CTX VOI regions (Fig. 1c) were located mostly in the lateral frontal, lateral temporal, lateral and medial parietal, insular, and anterior striatal regions. The FBB-FMM CTX VOI regions also generally overlapped with the standard CTX VOI regions derived from PiB by Klunk et al. (Supplementary eFig. 1) [11].

We generated FBB and FMM dcSUVR using the FBB-FMM CTX VOI template. The paired FBB and FMM dcSUVR values demonstrated excellent linear correlation (Fig. 2a; $R^2 = 0.97$, FMM dcSUVR = $0.99 \times$ FBB dcSUVR + 0.01), with a slope of 0.99. The paired FBB and FMM SUVR_{standard} values also correlated highly when using the standard CTX VOI (Fig. 2b; $R^2 = 0.97$, FMM SUVR_{standard} = $1.00 \times$ FBB SUVR_{standard} + 0.004), with a slope of 1.00.

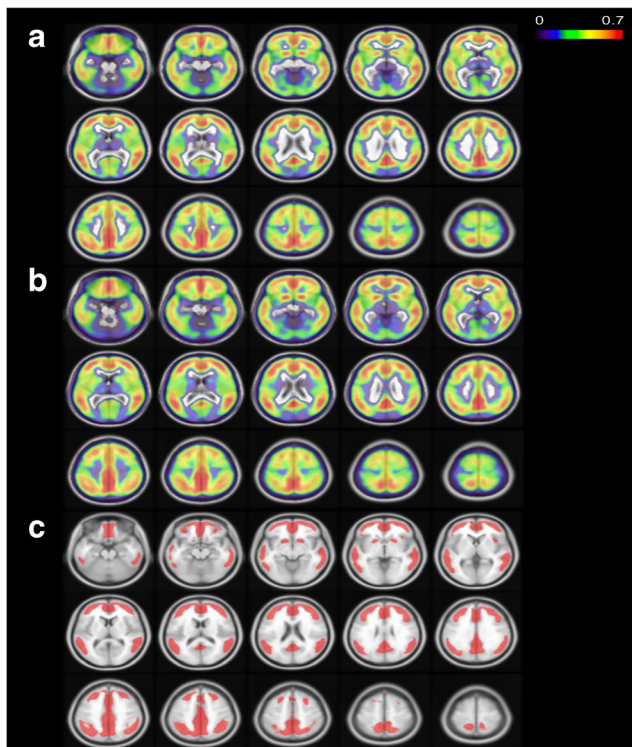


Fig. 1 Increased amyloid uptake region in ADICI participants compared to OCs in **a** FBB, **b** FMM, and **c** CTX VOI. **a** and **b** show regions in which ADICI participants had higher SUVR differences than OCs for FBB and FMM, respectively. The scale bar indicates SUVR differences between ADICI participants and OCs. **c** Our FBB-FMM CTX VOI (red areas), defined as AD-specific cortical target regions in FBB and FMM, contains voxels in the upper 20% intensity in the intersecting images, common to both FBB and FMM. The regions are mapped on an MNI 152 template. ADICI, Alzheimer's disease-related cognitive impairment; OCs, old controls; FBB, ^{18}F -florbetaben; FMM, ^{18}F -flutemetamol; CTX VOI, global cortical target volume of interest

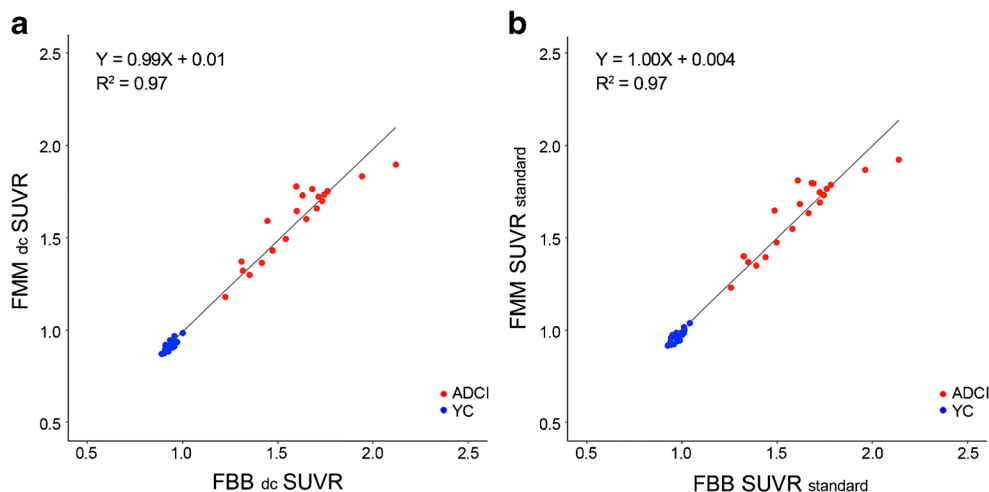


Fig. 2 Plots of paired FBB and FMM SUVR values calculated using our method and the standard method. SUVR correlations for YC and ADICI participants with **a** our direct comparison (dc) method using the FBB-FMM CTX VOI and **b** the standard method using the standard CTX VOI (both with reference to the whole cerebellum) are shown as scatterplots.

Conversion of FMM SUVR and FBB SUVR into CL units

We used our direct comparison of FBB-FMM method to derive equations to convert the FBB dcSUVR into FBB dcCL (Fig. 3a) and the FMM dcSUVR into FMM dcCL (Fig. 3b). By setting the mean YC SUVR as 0 CL and the mean ADICI SUVR as 100 CL for each tracer, we calculated the regression equations presented in Fig. 3a ($\text{FBB dcCL} = 151.42 \times \text{FBB dcSUVR} - 142.24$) and Fig. 3b ($\text{FMM dcCL} = 148.52 \times \text{FMM dcSUVR} - 137.09$).

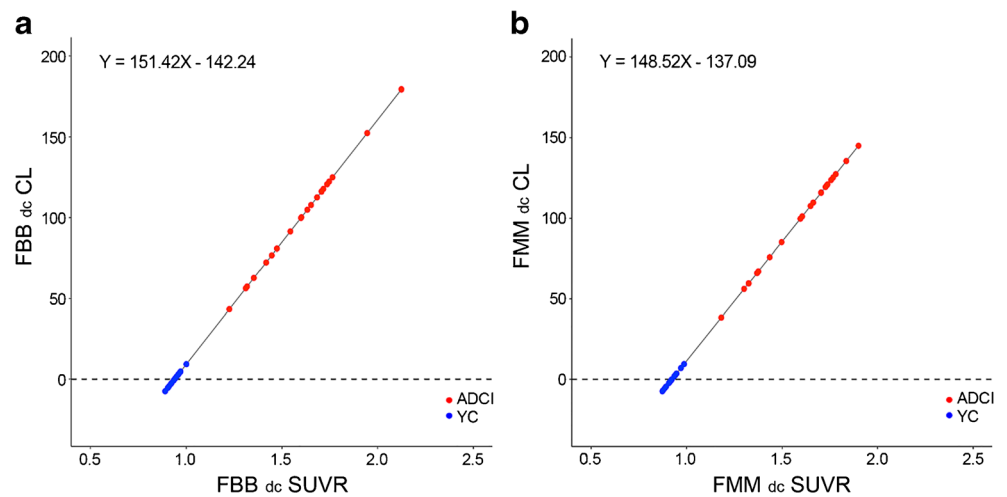
The correlation between the SUVR and CL values from the standard method using the standard CTX VOI was obtained by applying the existing published equations to FBB ($\text{FBB CL}_{\text{standard}} = 153.4 \times \text{FBB SUVR}_{\text{standard}} - 154.9$) [6] and FMM ($\text{FMM CL}_{\text{standard}} = 121.42 \times \text{FMM SUVR}_{\text{standard}} - 121.16$) [7].

Reliability and precision in the new and standard CL methods

For reliability, we investigated the correlation between the FBB and FMM CL values calculated using the two CL methods. With our direct comparison of FBB-FMM method, the dcCL units between FBB and FMM were highly correlated ($R^2 = 0.97$, $\text{FMM dcCL} = 0.97 \times \text{FBB dcCL} + 1.64$) (Fig. 4a). The CL_{standard} units between FBB and FMM were also highly correlated using the standard method ($R^2 = 0.97$, $\text{FMM CL}_{\text{standard}} = 0.79 \times \text{FBB CL}_{\text{standard}} + 1.36$) (Fig. 4b).

For precision, we investigated the CL unit difference between FBB and FMM calculated using the direct comparison (Fig. 5a) and standard methods (Fig. 5b). The GEE showed that the absolute CL value differences

Fig. 3 Plots of SUVR values and direct comparison of FBB-FMM CL (dcCL) units for FBB and FMM using the FBB-FMM CTX VOI. SUVR values, dcCL units, and the SUVR translation equation to dcCL for both **a** FBB and **b** FMM using the FBB-FMM CTX VOI are shown as scatterplots. ADCI, Alzheimer’s disease-related cognitive impairment; YC, young control; FBB, ¹⁸F-florbetaben; FMM, ¹⁸F-flutemetamol; SUVR, standardized uptake value ratio; CL, Centiloid; CTX VOI, global cortical target volume of interest



between FBB and FMM were smaller with our dcCL method (6.16 ± 1.01 , mean \pm standard error) than with the standard CL method (10.22 ± 1.53) ($P = 0.01$). We also investigated the CL unit difference between our dcCL method and the standard method for FBB (Fig. 5c) and FMM (Fig. 5d). The GEE showed that the absolute CL value differences between the our dcCL and the standard method were smaller for FBB CL (5.65 ± 0.74) than for FMM CL (13.69 ± 0.99) ($P < 0.001$). In particular, FMM showed increased differences to 30 CL between the dcCL method and the standard method, according to the increased mean CL of the dcCL and standard methods (Fig. 5d). To improve understanding of the reliability and precision of the CL methods, we have summarized all the measured SUVRs and associated CL values in Supplementary eTable 1.

Effect size of CL between ADCI and YC participants and CL variance in YCs

Table 2 shows the summary statistics for the FBB and FMM CL values from both our method and the standard method. With our dcCL calculation method, the effect sizes of dcCL between the ADCI and YC participants were 4.07 in FBB and 4.53 in FMM. The dcCL variances in the YCs were 4.23 in FBB and 4.31 in FMM. There were no significant differences in the dcCL variances in the YCs between FBB and FMM ($P = 0.86$).

With the standard CL method, the effect sizes of CLstandard between the ADCI participants and YCs were 4.04 in FBB and 4.57 in FMM. The CLstandard variances in the YCs were 4.66 in FBB and 3.88 in FMM. There were no significant differences in the CLstandard variances in the YCs between FBB and FMM ($P = 0.26$).

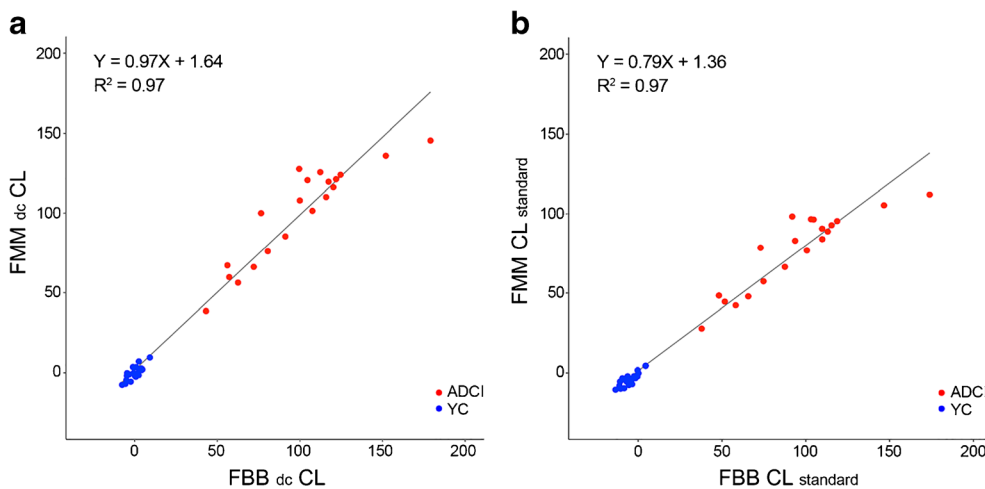


Fig. 4 Plots of paired FBB and FMM CL units calculated using our direct comparison of FBB-FMM method and the standard method. Centiloid values for FBB and FMM using **a** our direct comparison of FBB-FMM CL method from FBB-FMM CTX VOI (dcCL) and **b** the standard

method from the standard CTX VOI (CLstandard) are shown as scatterplots. ADCI, Alzheimer’s disease-related cognitive impairment; YC, young control; FBB, ¹⁸F-florbetaben; FMM, ¹⁸F-flutemetamol; CL, Centiloid; CTX VOI, global cortical target volume of interest

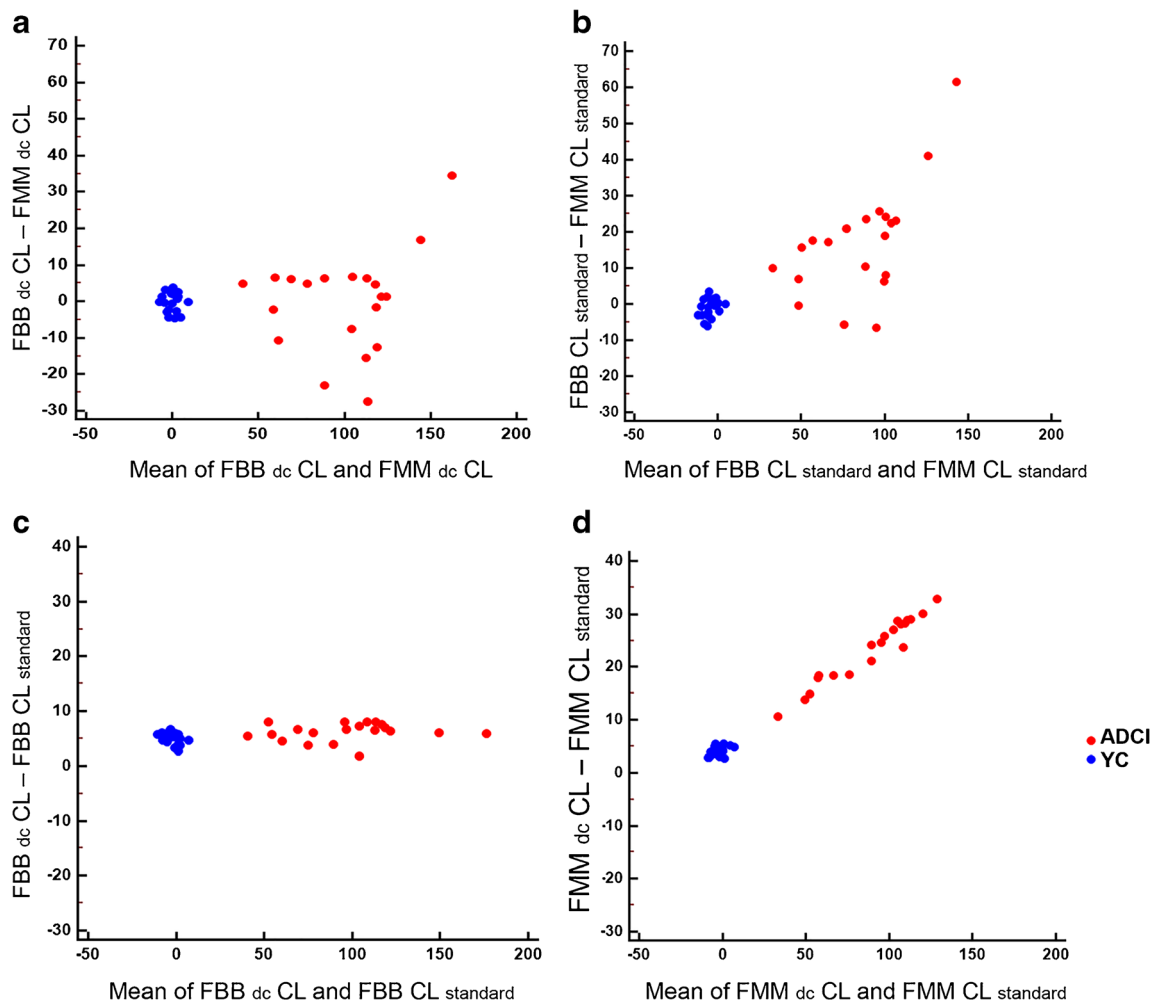


Fig. 5 The patterns of difference between FBB and FMM Centiloid (CL) values calculated using the direct comparison of FBB-FMM method (dcCL) and the standard method (CLstandard). We visualize the agreement between FBB CL and FMM CL values using **a** the direct comparison of FBB-FMM method and **b** the standard method. We also

visualize the agreement between the direct comparison of FBB-FMM method and the standard method separated by **c** FBB CL and **d** FMM CL. ADCI, Alzheimer's disease-related cognitive impairment; YC, young control; FBB, ^{18}F -florbetaben; FMM, ^{18}F -flutemetamol; CL, Centiloid

Table 2 Summary statistics of SUVR and Centiloid (CL) units from our direct comparison of FBB-FMM CL (dcCL) method and standard method

		FBB-FMM CTX VOI				Standard CTX VOI			
		FBB		FMM		FBB		FMM	
		dcSUVR	dcCL	dcSUVR	dcCL	SUVR _{standard}	CL _{standard}	SUVR _{standard}	CL _{standard}
ADCI	Mean	1.60	100	1.60	100	1.62	93.80	1.63	75.75
	SD	0.22	33.63	0.20	30.12	0.22	33.39	0.20	24.11
YC	Mean	0.94	0.00	0.92	0.00	0.98	-5.10	0.96	-4.14
	SD	0.03	4.23	0.03	4.31	0.03	4.66	0.03	3.88
Effect size		4.07	4.07	4.53	4.53	4.04	4.04	4.57	4.57

FBB, ^{18}F -florbetaben; FMM, ^{18}F -flutemetamol; CTX VOI, global cortical target volume of interest; SUVR, standardized uptake value ratio; CL, Centiloid; dcSUVR, SUVR derived from FBB-FMM CTX VOI; dcCL, CL unit derived using our direct comparison of FBB-FMM method from the regression equations to FBB (FBB dcCL = $151.42 \times \text{FBB dcSUVR} - 142.24$) and FMM (FMM dcCL = $148.52 \times \text{FMM dcSUVR} - 137.09$); SUVR_{standard}, SUVR derived from standard CTX VOI; CL_{standard}, CL unit derived by applying the existing published equations to FBB (FBB CL_{standard} = $153.4 \times \text{FBB SUVR}_{\text{standard}} - 154.9$) [6] and FMM (FMM CL_{standard} = $121.42 \times \text{FMM SUVR}_{\text{standard}} - 121.16$) [7]; ADCI, Alzheimer's disease-related cognitive impairment; YC, young control; SD, standard deviation

Discussion

We performed head-to-head comparisons of the FBB and FMM A β imaging tracers in ADICI, OC, and YC groups using CL units calculated directly from new FBB-FMM SUVRs (without conversion to the PiB SUVR) and those calculated using the standard CL method, which involves translation to and from the PiB SUVR. In the present study, our direct comparison of FBB-FMM CL method and the previous standard method produced FBB and FMM CL units that were highly correlated. However, the CL variation between FBB and FMM was smaller with our direct conversion method than with the previous conventional method. Taken together, our findings suggest that it is reasonable to convert FBB or FMM SUVR values into the CL scale directly rather than using the classical method, at least in environments where FBB or FMM ligands are used frequently. Furthermore, giving researchers access to diverse specific CL methods that they can apply in a variety of conditions might provide clinicians with better diagnostic and prognostic data that are applicable to all A β PET scans.

We found that the spatial distribution of increased FMM uptake was similar to that of FBB. Specifically, the FBB-FMM CTX VOI regions were mostly located in the lateral frontal, lateral temporal, lateral and medial parietal, insular, and anterior striatal regions, which are known to be vulnerable to amyloid deposition [3]. These regions also generally overlapped with the standard CTX VOI regions [11], with the involvement of the anterior striatum and insular cortex. According to the Thal stages, amyloid deposition occurs first in the isocortical cortex (Thal stage 1), followed by the allocortical insular cortex (Thal stage 2) and the striatum (Thal stage 3) [25]. Previous research examining florbetapir explored removing the anterior striatum and insular cortex from the CTX VOI because of concerns about nonspecific binding and partial volume effects, but no differences were found when these regions were excluded [13]. Our findings suggest that both FBB and FMM can detect amyloid burden in Thal stages 2 and 3.

In the present study, FMM dcSUVR seemed to have a similar dynamic range FBB dcSUVR. In previous head-to-head studies, FMM SUVR seemed to have a slightly higher dynamic range than FBB SUVR, with a slope of 0.71 for FBB-PiB [26] and 0.80 for FMM-PiB [27]. This discrepancy could be explained by the use of different cortical target regions and the different equipment between our present study and the previous head-to-head comparison studies. Specifically, there were differences in the cortical target regions (frontal, superior parietal, lateral temporal, lateral occipital, and anterior and posterior cingulate in the FBB-PiB study [26] and frontal, parietal, lateral temporal, precuneus, and anterior cingulate in the FMM-PiB study [27]) and the kinds of scanners

(Philips PET camera/scanner for both PiB and FBB PET [26] and Siemens scanner for PiB and FMM PET [27]). However, in this study, we used the same cortical target region (FBB-FMM CTX VOI) and the same equipment (GE PET scanner). Further studies directly comparing the F ligands need to be done to validate our results.

Our major finding is that although the FBB and FMM CL values were highly correlated using both our direct comparison of FBB-FMM CL method and the previous standard method, the CL value differences between FBB and FMM were smaller with our CL method (6.16) than with the standard CL method (10.22). In terms of reliability, not only is our new method similar to the standard method, but also the CL calculated with our new method might also generate more precise values than those produced by the standard method. The translation of FBB and FMM SUVR values into CL units via equations defined using PiB might be affected by unique characteristics of the PiB ligand, which could have cascading effects on the precision of the downstream FBB and FMM CL values. Our findings therefore suggest that it might be more appropriate to apply a direct one-step conversion process when comparing CL values between ^{18}F -labeled tracers, rather than a two-step conversion process via PiB, particularly in settings such as ours, in which FBB and FMM, but not PiB, are commonly used.

Our findings have some clinical implications. Although the standard CL method was developed to harmonize different tracers, it is important to maintain the true precision of each tracer. Furthermore, the ^{18}F ligands are replacing PiB in many multicenter studies because the short half-life (20 min) of [^{11}C] PiB limits its widespread use. Therefore, studies using exclusively ^{18}F -labeled tracers will soon require a variety of direct one-step CL conversion processes among the ^{18}F -labeled tracers to directly compare the amyloid burden reported by each.

We also found differences in the slopes of FBB and FMM CL values between our direct comparison method and the standard method; whereas the direct comparison method had a slope near one, the standard method produced a slope near 0.79. Considering that the slopes of the FBB SUVR to FMM SUVR were near one in both our FBB-FMM CTX VOI and the standard CTX VOI, it is reasonable to conclude that the standard two-step process for converting FBB and FMM SUVRs into CL units via PiB caused differences in the slopes. Alternatively, our finding might be related to the effects of different cameras on the development of standard F-ligands in the CL conversion equation. In the present study, we conducted FBB and FMM PET using the same type of scanner (GE Medical Systems, Milwaukee, WI, USA). However, when developing the standard F-ligand CL conversion equations, the researchers used the different scanners for different F-ligands (a Philips PET camera/scanner for PiB and FBB PET [6] and Siemens and GE scanners for PiB and FMM

PET [7]). In a previous FMM CL study [7], participants were taken from previous studies of paired PiB and FMM PET scans taken using GE PET/CT scanners [28] and GE and Siemens scanners, at different sites with different machines [29]. In fact, in the present study, the mean ADCI CL standard unit of FBB was 93.80 for the standard CTX VOI, whereas the mean ADCI CL standard unit of FMM was only 75.75 for the standard CTX VOI. Also, when comparing the differences in CLs between our method and the standard method for each ligand, the FMM CLs tended to be more underestimated in the standard method than in our new method, especially as they increased, whereas the FBB CLs seemed to be stable in both the standard and new methods regardless of their level. It is therefore possible that camera differences might affect the development of a standard F-ligand CL conversion equation. Further studies with more cases are needed to determine whether that is, in fact, the case.

Our conclusion, that our method produces FBB dcCL and FMM dcCL values that are interchangeable with each other for clinical and research applications, is supported by the following observations. First, FBB dcCL correlated highly with FMM dcCL. The correlation coefficient (R^2) between FBB dcCL and FMM dcCL was 0.97. The study originally defining CL [11] said that well-correlated tracers/methods should have an R^2 of > 0.7 . Second, the variability observed in the YC group provides an estimate of the relative precision of the two tracers, and there were no differences in the CL variance in the YCs between FBB (4.23) and FMM (4.31). Previous studies have suggested that ^{18}F -labeled ligands had larger variances of CL in YCs (6.81 for FBB [6] and 7.2 for FMM [7]) than PiB (4.34) [11]. However, the CL variance in YCs from our method was comparable with that reported for PiB. Finally, the effect size of CL did not differ between FBB (4.07) and FMM (4.55) and was comparable with previous results. The previously reported effect size for FBB SUVR was 3.0 [26], and PiB was reported to have various effect sizes (3.3, 4.50, and 7.14) [11, 23, 26].

Our study has the advantage of directly comparing the FBB and FMM ligands in a single group of YC, OC, and ADCI participants, allowing us to compare the characteristics of the two tracers directly under a variety of conditions. Also, we validated our data against the GAAIN data and found excellent correlations that fulfilled the required acceptance criteria [11]. Nonetheless, our study has several limitations. First, it would have been best if we had done PiB PET, as well as FBB and FMM PET, but it was not possible to scan participants with all three ligands. We know of no head-to-head studies translating SUVR values into CL units for all three ligands in the same participants. Second, this result might be difficult to apply to other settings in which $\text{A}\beta$ PET is acquired because differences between $\text{A}\beta$ PET imaging systems and reconstruction methods at other sites could affect the results. Third, the

older age of our OC group relative to the ADCI group might have caused a reduction in the FBB-FMM CTX VOI voxels. Fourth, we were unable to evaluate correlations between postmortem pathology and CL units. Fifth, we did not evaluate test-retest variation. Further work performing cross-tracer comparisons is needed. Finally, while we chose to select high-retention regions for both ligands, more work could be done to optimize and standardize the threshold for the FBB-FMM CTX VOI. Despite those limitations, our findings provide a mechanism for comparing different $\text{A}\beta$ tracers, FBB and FMM in this case, on a unified scale in a standard manner. The design and implementation of CL methods that can quantify and compare $\text{A}\beta$ PET imaging results in multiple potential research settings is an important step toward better and more standardized clinical and research use of $\text{A}\beta$ imaging.

Conclusions

Our direct comparison of FBB-FMM CL method showed more precision than the standard method and enables FBB and FMM results to be interchangeable. This will allow the use of multiple $\text{A}\beta$ tracers in multicenter trials of anti- $\text{A}\beta$ therapies using ^{18}F -labeled ligands. Future studies are warranted to assess how well this standardization method improves desired cross-tracer comparisons, especially the delineation of amyloid-negative scan values and amyloid loads associated with clinical dementia, the ease of cross-study/cross-site comparisons, and use within longitudinal settings.

Author contributions S.H.C., Y.S.C., and S.W.S. contributed to the conceptualization of the study, analysis and interpretation of data, and drafting. Y.S.C. and S.B.P. contributed to analyses of imaging data, prepared the figures, and provided technical support. B.C.K., H.J.K., H.M.J., Y.S.K., S.E.K., S.J.K., J.P.K., Y.H.J., and D.L.N. contributed to the interpretation of data. S.L.B. and S.N.L. drafted the manuscript.

Funding information This research was supported by a National Research Foundation of Korea grant funded by the Korean government (MSIP) (No. NRF-2017R1A2B2005081) and by Research of Korea Centers for Disease Control and Prevention (No. 2018-ER6203-01).

Compliance with ethical standards

Conflict of interest The authors declare that they have no conflict of interest.

Disclaimer The funders had no role in the design and conduct of the study; collection, management, analysis, and interpretation of the data; preparation, review, or approval of the manuscript; or decision to submit the manuscript for publication.

Ethical approval All procedures performed in studies involving human participants were in accordance with the ethical standards of the institutional and/or national research committee and with the 1964 Helsinki declaration and its later amendments or comparable ethical standards.

Informed consent Informed consent was obtained from all individual participants included in the study.


References

- Klunk WE, Engler H, Nordberg A, Wang Y, Blomqvist G, Holt DP, et al. Imaging brain amyloid in Alzheimer's disease with Pittsburgh Compound-B. *Ann Neurol*. 2004;55:306–19.
- Wong DF, Rosenberg PB, Zhou Y, Kumar A, Raymont V, Ravert HT, et al. In vivo imaging of amyloid deposition in Alzheimer disease using the radioligand 18F-AV-45 (florbetapir [corrected] F 18). *J Nucl Med*. 2010;51:913–20.
- Barthel H, Gertz HJ, Dresel S, Peters O, Bartenstein P, Buerger K, et al. Cerebral amyloid-beta PET with florbetaben (18F) in patients with Alzheimer's disease and healthy controls: a multicentre phase 2 diagnostic study. *Lancet Neurol*. 2011;10:424–35.
- Rinne JO, Wong DF, Wolk DA, Leinonen V, Arnold SE, Buckley C, et al. [(18F)] Flutemetamol PET imaging and cortical biopsy histopathology for fibrillar amyloid beta detection in living subjects with normal pressure hydrocephalus: pooled analysis of four studies. *Acta Neuropathol*. 2012;124:833–45.
- Landau SM, Thomas BA, Thurfjell L, Schmidt M, Margolin R, Mintun M, et al. Amyloid PET imaging in Alzheimer's disease: a comparison of three radiotracers. *Eur J Nucl Med Mol Imaging*. 2014;41:1398–407.
- Rowe CC, Dore V, Jones G, Baxendale D, Mulligan RS, Bullich S, et al. (18F)-Florbetaben PET beta-amyloid binding expressed in Centiloids. *Eur J Nucl Med Mol Imaging*. 2017;44:2053–9.
- Battle MR, Pillay LC, Lowe VJ, Knopman D, Kemp B, Rowe CC, et al. Centiloid scaling for quantification of brain amyloid with [(18F)] flutemetamol using multiple processing methods. *EJNMMI Res*. 2018;8:107.
- Carbonell F, Zijdenbos AP, Charil A, Grand'Maison M, Bedell BJ. Optimal target region for subject classification on the basis of amyloid PET images. *J Nucl Med*. 2015;56:1351–8.
- Landau SM, Fero A, Baker SL, Koeppe R, Mintun M, Chen K, et al. Measurement of longitudinal beta-amyloid change with 18F-florbetapir PET and standardized uptake value ratios. *J Nucl Med*. 2015;56:567–74.
- Tudorascu DL, Minhas DS, Lao PJ, Bethausen TJ, Yu Z, Laymon CM, et al. The use of Centiloids for applying [(11C)] PiB classification cutoffs across region-of-interest delineation methods. *Alzheimers Dement (Amst)*. 2018;10:332–9.
- Klunk WE, Koeppe RA, Price JC, Benzinger TL, Devous MD Sr, Jagust WJ, et al. The Centiloid Project: standardizing quantitative amyloid plaque estimation by PET. *Alzheimers Dement*. 2015;11:1-15.e1-4.
- Villemagne VL, Burnham S, Bourgeat P, Brown B, Ellis KA, Salvado O, et al. Amyloid beta deposition, neurodegeneration, and cognitive decline in sporadic Alzheimer's disease: a prospective cohort study. *Lancet Neurol*. 2013;12:357–67.
- Navitsky M, Joshi AD, Kennedy I, Klunk WE, Rowe CC, Wong DF, et al. Standardization of amyloid quantitation with florbetapir standardized uptake value ratios to the Centiloid scale. *Alzheimers Dement*. 2018;14:1565–71.
- Park JH, Seo SW, Kim C, Kim GH, Noh HJ, Kim ST, et al. Pathogenesis of cerebral microbleeds: in vivo imaging of amyloid and subcortical ischemic small vessel disease in 226 individuals with cognitive impairment. *Ann Neurol*. 2013;73:584–93.
- McKhann GM, Knopman DS, Chertkow H, Hyman BT, Jack CR Jr, Kawas CH, et al. The diagnosis of dementia due to Alzheimer's disease: recommendations from the National Institute on Aging-Alzheimer's Association workgroups on diagnostic guidelines for Alzheimer's disease. *Alzheimers Dement*. 2011;7:263–9.
- Petersen RC, Smith GE, Waring SC, Ivnik RJ, Tangalos EG, Kokmen E. Mild cognitive impairment: clinical characterization and outcome. *Arch Neurol*. 1999;56:303–8.
- Kim HJ, Yang JJ, Kwon H, Kim C, Lee JM, Chun P, et al. Relative impact of amyloid-beta, lacunes, and downstream imaging markers on cognitive trajectories. *Brain*. 2016;139:2516–27.
- Jang H, Jang YK, Kim HJ, Werring DJ, Lee JS, Choe YS, et al. Clinical significance of amyloid beta positivity in patients with probable cerebral amyloid angiopathy markers. *Eur J Nucl Med Mol Imaging*. 2019;46:1287–98.
- Kim SE, Woo S, Kim SW, Chin J, Kim HJ, Lee BI, et al. A nomogram for predicting amyloid PET positivity in amnesic mild cognitive impairment. *J Alzheimers Dis*. 2018;66:681–91.
- Barthel H, Bullich S, Sabri O, Seibyl J, Villemagne V, Rowe C, et al. 18F-Florbetaben (FBB) PET SUVR quantification: which reference region? *J Nucl Med*. 2015;56:1563.
- Farrar G. Regional visual read inspection of [18F]flutemetamol brain images from end-of-life and amnesic MCI subjects. *J Nucl Med*. 2017;58:1250.
- Sled JG, Zijdenbos AP, Evans AC. A nonparametric method for automatic correction of intensity nonuniformity in MRI data. *IEEE Trans Med Imaging*. 1998;17:87–97.
- Yun HJ, Moon SH, Kim HJ, Lockhart SN, Choe YS, Lee KH, et al. Centiloid method evaluation for amyloid PET of subcortical vascular dementia. *Sci Rep*. 2017;7:16322.
- Bland JM, Altman DG. Statistical methods for assessing agreement between two methods of clinical measurement. *Lancet*. 1986;1:307–10.
- Serrano-Pozo A, Frosch MP, Masliah E, Hyman BT. Neuropathological alterations in Alzheimer disease. *Cold Spring Harb Perspect Med*. 2011;1:a006189.
- Villemagne VL, Mulligan RS, Pejoska S, Ong K, Jones G, O'Keefe G, et al. Comparison of 11C-PiB and 18F-florbetaben for Abeta imaging in ageing and Alzheimer's disease. *Eur J Nucl Med Mol Imaging*. 2012;39:983–9.
- Mountz JM, Laymon CM, Cohen AD, Zhang Z, Price JC, Boudhar S, et al. Comparison of qualitative and quantitative imaging characteristics of [11C]PiB and [18F]flutemetamol in normal control and Alzheimer's subjects. *Neuroimage Clin*. 2015;9:592–8.
- Lowe VJ, Lundt E, Knopman D, Senjem ML, Gunter JL, Schwarz CG, et al. Comparison of [(18F)]Flutemetamol and [(11C)]Pittsburgh Compound-B in cognitively normal young, cognitively normal elderly, and Alzheimer's disease dementia individuals. *Neuroimage Clin*. 2017;16:295–302.

29. Vandenberghe R, Van Laere K, Ivanoiu A, Salmon E, Bastin C, Triau E, et al. 18F-flutemetamol amyloid imaging in Alzheimer disease and mild cognitive impairment: a phase 2 trial. *Ann Neurol*. 2010;68:319–29.

Publisher's note Springer Nature remains neutral with regard to jurisdictional claims in published maps and institutional affiliations.

Affiliations

Soo Hyun Cho^{1,2} · Yeong Sim Choe^{1,3,4} · Hee Jin Kim^{1,4} · Hyemin Jang^{1,4} · Yeshin Kim^{1,5} · Si Eun Kim^{1,6} · Seung Joo Kim^{1,7} · Jun Pyo Kim^{1,4} · Young Hee Jung^{1,8} · Byeong C. Kim² · Suzanne L. Baker⁹ · Samuel N. Lockhart¹⁰ · Duk L. Na^{1,3,4,11} · Seongbeom Park^{1,4} · Sang Won Seo^{1,3,4,12,13,14} 

¹ Department of Neurology, Samsung Medical Center, Sungkyunkwan University School of Medicine, Seoul, Korea

² Department of Neurology, Chonnam National University Hospital, Chonnam National University Medical School, Gwangju, Korea

³ Department of Health Sciences and Technology, SAIHST, Sungkyunkwan University, Seoul, Korea

⁴ Neuroscience Center, Samsung Medical Center, Seoul, Korea

⁵ Department of Neurology, Kangwon National University Hospital, Kangwon National University College of Medicine, Chuncheon, Korea

⁶ Department of Neurology, Inje University College of Medicine, Haeundae Paik Hospital, Busan, Korea

⁷ Department of Neurology, Gyeongsang National University School of Medicine and Gyeongsang National University Changwon Hospital, Changwon, Korea

⁸ Department of Neurology, Myoungji Hospital, Hanyang University, Goyangsi, Korea

⁹ Molecular Biophysics and Integrated Bioimaging, Lawrence Berkeley National Laboratory, Berkeley, CA, USA

¹⁰ Internal Medicine - Gerontology and Geriatric Medicine, Wake Forest School of Medicine, Winston-Salem, NC, USA

¹¹ Stem Cell & Regenerative Medicine Institute, Samsung Medical Center, Seoul, Korea

¹² Department of Clinical Research Design & Evaluation, SAIHST, Sungkyunkwan University, Seoul, Korea

¹³ Samsung Alzheimer Research Center, Samsung Medical Center, Seoul, Korea

¹⁴ Center for Clinical Epidemiology, Samsung Medical Center, Seoul, Korea